

Contribution to the Radio Light Curves of a Core-Collapse Supernova due to the Off-axis Gamma-Ray Burst Afterglow

YO KUSAFUKA ¹, TOMOKI MATSUOKA ² AND RYO SAWADA ¹

¹*Institute for Cosmic Ray Research, The University of Tokyo, Kashiwa, Chiba 277-8582, Japan*

²*Institute of Astronomy and Astrophysics, Academia Sinica, No.1, Sec. 4, Roosevelt Road, Taipei 106216, Taiwan*

(Received March 18, 2025)

Submitted to ApJL

ABSTRACT

We present the first comprehensive theoretical predictions of radio emission from a Type Ic-BL supernova (SN) associated with a gamma-ray burst (GRB) jet. It is naturally supposed that the expected radio light curve consists of two components of emitting source: radio emission from a non-relativistic SN shock and afterglow emitted from the head of the relativistic GRB jet. We calculate each component of radio emission, placing an emphasis on surveying wide ranges of isotropic explosion energy and viewing angle in our GRB afterglow modeling. We show that in particular parameter space, the composite radio light curve would be characterized by a double-peaked shape. The condition for the clear appearance of the double-peaked radio light curve is either (1) the isotropic explosion energy is small (low-luminosity GRB) or (2) the viewing angle is large (off-axis GRB). Our results highlight that follow-up radio observations conducted within a few years after the optical discovery of nearby Type Ic-BL supernovae (~ 100 Mpc) can serve as a unique diagnostic for off-axis GRBs undiscovered in Type IcBL SNe. This will be a step toward uncovering the nature of long GRB progenitors and clarifying their connection to Type IcBL SNe.

1. INTRODUCTION

The connection between long gamma-ray bursts (long GRBs) and broad-lined hydrogen/helium-deficient supernovae (Type Ic-BL SNe) was first established by the discovery of GRB 980425 and its associated SN 1998bw (Kulkarni et al. 1998; Galama et al. 1999). Over the past quarter-century, substantial observational efforts have revealed at least 61 confirmed GRB-SN associations (see Wang & Wheeler 1998; Woosley & Bloom 2006; Cano et al. 2017; Finneran et al. 2024). All of these SNe share the characteristic spectral classification of Type Ic-BL, distinguished by their lack of hydrogen and helium absorption features and unusually broad spectral lines indicative of high ejecta velocities (e.g., Woosley & Bloom 2006). However, despite the increase in observational samples of Type Ic-BL SNe, it remains unclear what proportion of all Type Ic-BL supernovae are intrinsically associated with GRBs (Finneran et al. 2024). The

number of GRB-SNe with their clear association is reported to be much lower than that of the observed Type IcBL SNe. The reasons for this discrepancy include (1) only a fraction of Type IcBL SNe intrinsically are associated with GRB events (Soderberg et al. 2006), (2) we can observe only events with successful penetration of the jet from the progenitor surface as GRB-SNe; otherwise, the jet is choked in the progenitor (MacFadyen et al. 2001; Ramirez-Ruiz et al. 2002), and (3) we are missing GRBs in Type IcBL SNe with the orientations of their jets out of our line of sight (off-axis GRB, but see also Izzo et al. 2020). In the third case, particularly, the emission from off-axis GRBs tends to be fainter than that of on-axis GRBs in the early phase (Granot et al. 2002). It is also the case that the small opening angle of GRB jets leads to a probably large population of off-axis GRBs compared to on-axis GRBs (Rossi et al. 2002). These properties make it difficult to give constraints on the intrinsic event rate of GRB-SN association, unlike the case of the occurrence rate of core-collapse SNe (van den Bergh & Tammann 1991).

Radio observations have been employed to investigate the intrinsic association between SNe and GRBs. Radio emission from SNe typically arises from the interaction between non-relativistic SN ejecta and circumstellar material (CSM) surrounding the progenitor star (Chevalier 1982a; Chevalier et al. 2006; Maeda 2012; Chevalier & Fransson 2017; Matsuoka et al. 2019). Afterglow emission from GRBs is produced in a wide range of wavelengths including radio as their relativistic jets decelerate by interacting with the ambient medium. It is shown that afterglow emission can leave distinctive signatures even for observers with their line of sight out of the opening angle of GRB jets (Granot et al. 2002). Radio emission survey of local Type Ibc SNe in the late phase ($\gtrsim 1$ year) after the optical discovery gave stringent constraints on the presence of off-axis GRB jets (Soderberg et al. 2006); they found that (1) less than approximately 10% of Type Ibc SNe could harbor GRB jets, and (2) it is ruled out with a high confidence level that every broad-lined SN is associated with a GRB jet. On the other hand, Soderberg et al. (2010) suggested that a search for bright radio emission in Type Ibc SNe driven by relativistic outflow would be a useful method to recover the presence of the GRB even without the detections of gamma-ray emission. Corsi et al. (2016) gave an upper limit on the fraction of Type IcBL SNe harboring an off-axis GRB jet based on SN samples discovered in Palomar Transient Factory and monitored by Very Large Array. In addition to these surveys, there are several studies on radio light curves of individual Type IcBL SNe to explore the presence of the signature of GRB jets, but their conclusions widely vary (see SN 2007bg for Salas et al. (2013), SN 2007uy for van der Horst et al. (2011), and PTF11qej for Palliyaguru et al. (2021)).

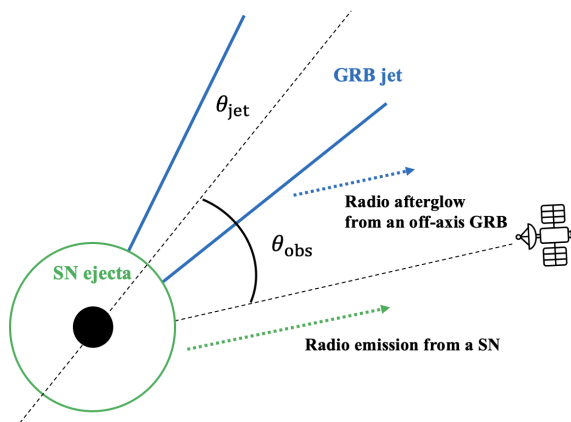


Figure 1. Schematic picture of the system assumed in this study.

Given the importance of radio observations, it would be critical to construct comprehensive and consistent theoretical modeling of combined SN-GRB radio emission. This study presents theoretical predictions of radio light curves that, for the first time, consistently incorporate both SN and GRB radio emissions. We explore wide ranges of GRB’s isotropic explosion energy and viewing angle—including the case of off-axis GRBs—to investigate the time evolution of composite radio emissions from GRB-SN systems (see Figure 1). Our approach aims not only to elucidate the intrinsic connection between Type IcBL SNe and GRBs but also to establish observational strategies for identifying elusive radio signatures of off-axis GRBs.

This paper is organized as follows. In Section 2, we describe our treatment of each component, focusing on the consistency caveats in the calculation of the SN and GRB components. In Section 3, we show the resulting radio light curves, and in particular, we show the response of the multi-peak signature to the observing angle and the energy of the GRB. In Section 4, we discuss the observational strategy, and summarize our results.

2. MODEL AND METHOD

In this study, we consider two shock waves of SN and GRB ejecta propagating in the same environment characterized by stellar wind of a progenitor star. We consider the density structure of CSM as

$$n_{\text{CSM}}(r) = 3 \times 10^{35} A r^{-2} \text{ cm}^{-3}, \quad (1)$$

where $A = (\dot{M}/10^{-5} M_{\odot}\text{yr}^{-1})(v_{\text{wind}}/10^3 \text{ km s}^{-1})^{-1}$ reflects the wind mass-loss rate of a typical Wolf-Rayet star (Maeda 2012; Suzuki & Maeda 2018).

Around shock waves, electrons are accelerated through diffusive shock acceleration (Blandford & Ostriker 1978; Bell 1978), magnetic reconnection (Sironi & Spitkovsky 2011; Sironi et al. 2015), or turbulent acceleration (Asano & Terasawa 2009; Asano et al. 2014). The injection rate of comoving spectral number density is described as a single power of the Lorentz factor γ of electrons: $Q(\gamma) \propto \gamma^{-p}$, ($\gamma_{\text{m}} \leq \gamma \leq \gamma_{\text{M}}$) (Sari et al. 1998). The theoretical prediction of the spectral index is $p = 2$ for non-relativistic shocks (Blandford & Ostriker 1978; Bell 1978) or $p \sim 2.2$ for relativistic shocks (Keshet & Waxman 2005). However, the inferred value of the observed radio SNe and GRBs afterglow suggest $2 < p < 3$ (Chevalier et al. 2006; Ryan et al. 2020). In this study, we use fixed values (see Section 3). We leave the difference in the spectral index p between the SNe and the GRB afterglow model.

The minimum Lorentz factor γ_{m} are computed as

$$\gamma_{\text{m}} = \begin{cases} \epsilon_e \frac{p-2}{p-1} \frac{m_p}{m_e} (\Gamma_{\text{sh}} - 1) & \text{(for GRB)} \\ 2 & \text{(for SN)} \end{cases}, \quad (2)$$

where m_p and m_e are the proton and electron mass. We introduced a microphysics parameter ϵ_e (e.g. Sari et al. 1998; Ryan et al. 2020). For the GRB case, we need the Lorentz factor in the bulk of the shocked CSM Γ_{sh} . For SN, we assume $\gamma_m \sim 2$ in this study because the velocity of the SN shock is in a non-relativistic regime (Wei et al. (2023), but see also Matsuoka et al. (2024)). The maximum Lorentz factor is given by the balance of acceleration with the Bohm limit and synchrotron cooling: $\gamma_M = \sqrt{\frac{6\pi e}{\sigma_T B}}$ (Fan & Piran 2006), where σ_T is the Thomson scattering cross section and e is the elementary charge. A fraction ϵ_B of the internal energy density $\epsilon_{\text{sh}} = 4\Gamma_{\text{sh}}(\Gamma_{\text{sh}} - 1)n_{\text{CSM}}m_p c^2$ can be transferred to the turbulent magnetic field $B = \sqrt{8\pi\epsilon_B\epsilon_{\text{sh}}}$ (Sari et al. 1998).

The spectra of these non-thermal particles are modified by radiative cooling. The steady state particle distribution can be written as (Matsuoka et al. 2024)

$$n(\gamma) = Ct_{\text{cool}}(\gamma)\gamma^{-1} \max(\gamma, \gamma_m)^{1-p}, \quad (3)$$

where $t_{\text{cool}}(\gamma)$ is the total cooling time scale including synchrotron, inverse Compton, and adiabatic cooling (Fransson & Björnsson 1998; Matsuoka et al. 2019; Maeda et al. 2021; Björnsson 2022). The cooling break γ_c is determined by the balance of the radiative cooling time scale and the dynamical time scale (Matsuoka et al. 2024; Kusafuka & Asano 2024). The normalization factor C can be derived by assuming the balance between injection and cooling of relativistic electrons at any time (Fransson & Björnsson 1998; Matsuoka et al. 2024)

$$C = \begin{cases} \frac{4(p-1)\Gamma_{\text{sh}}n_{\text{CSM}}\Gamma_{\text{sh}}c}{\gamma_m^{1-p}R_{\text{sh}}} & \text{(for GRB)} \\ \frac{9(p-2)\epsilon_e n_{\text{CSM}}m_p V_{\text{sh}}^3}{8\gamma_m^{2-p}m_e c^2 \Delta R} & \text{(for SN)} \end{cases}, \quad (4)$$

where V_{sh} is the velocity of the shock surface.

We calculate synchrotron radiation and synchrotron self-absorption (SSA) using fitting formulae for the synchrotron function (Aharonian et al. 2010; Fouka & Ouichaoui 2013) under thin shell approximation. The shell width of the shocked wind is estimated as $\Delta R \equiv R_{\text{sh}}/(4\Gamma_{\text{sh}})$ for GRBs. Meanwhile, $\Delta R \equiv fR_{\text{sh}}$ is adopted for SNe, where f is the geometric thickness factor depending on the choice of n (Chevalier 1982b; Chevalier & Fransson 1994; Truelove & McKee 1999) (usually $f \sim 0.2$). To calculate the observed radio flux F_ν , we adopt the source distance as $D_L = 100$ Mpc and $z = 0.024$.

For GRB, we consider the Equal Arrival Time Surface (EATS) for the observed radiation flux (Waxman 1997; Granot 2005). To calculate the observed radiation flux from off-axis afterglows, we should integrate over the

solid angle along with EATS (Woods & Loeb 1999; Pang & Dai 2024). We take $\theta = 0$ as the line of sight. We don't consider the EATS effects for SNe because the speed of shock wave is non-relativistic.

2.1. The dynamics of GRBs afterglow

In this subsection, we describe the interaction between the wind and the cold top-hat jet with the initial Lorentz factor $\Gamma_0 = 100$, isotropic equivalent energy E_{iso} , and the opening angle $\theta_{\text{jet}} = 0.05$ rad. In general, the width of the ejecta and magnetization may modify the early phase evolution (Kobayashi & Sari 2000; Mimica et al. 2009; van Eerten 2014; Kusafuka et al. 2023; Kusafuka & Asano 2024). Since our interest in this study is the late afterglow, we simply neglected these effects.

We use the semi-analytic model given in Duffell & Laskar (2018), where we adopt $P_k = 2.0$ and $Q_k = 1.6$ in Eqs. (28), (29), (30), and (31) in their paper. In their model, the dynamics of the shock wave is characterized by 4 phases. At first, the dynamics of the shock in their model is a free expansion with constant Γ_0 until the deceleration radius $R_{\text{dec}} = E_{\text{iso}}/(4\pi n_{\text{CSM}}r^2 m_p c^2 \Gamma_0^2)$ (Sari & Piran 1995). Beyond R_{dec} , the shock decelerates adiabatically following the Blandford-McKee (BM) solution $\Gamma_{\text{sh}} \propto t^{-1/2}$ (Blandford & McKee 1976; Gianios et al. 2008; Gao et al. 2013). The dynamics of the shock wave is further modified after the causal connection around $\Gamma_{\text{sh}} \sim \theta_{\text{jet}}^{-1}$, starting lateral spreading (Rhoads 1999; van Eerten & MacFadyen 2012; Duffell & Laskar 2018; Ryan et al. 2020). Finally, the shock decelerates non-relativistic following the Sedov-Taylor solution $\Gamma_{\text{sh}}\beta_{\text{sh}} \propto t^{-1/3}$ (Ostriker & McKee 1988).

2.2. The dynamics of radio SNe

In this subsection, we describe the interaction between the wind and SN ejecta with the initial mass $M_{\text{ej}} = 1.5M_\odot$, the kinetic energy $E_{\text{ej}} = 4 \times 10^{51}$ erg (Young et al. 2010), and its density structure consisting of a flat inner component and a steep outer layer with a density slope $n = 7$ (Chevalier 1982a,b). We follow so-called thin-shell approximation where the thin shell consisting of the shocked CSM and the shocked ejecta is pushed outward by the ram pressure of the ejecta (Chevalier 1982a; Chevalier & Fransson 2017). Assuming that the location of the shock is almost the same as that of the thin shell, we can describe the explicit formula of the time evolution of the shock wave (for the concrete description, see Eqs. (4), (5), (6) in Matsuoka et al. 2024).

3. RESULTS

Based on the shock wave dynamics given in the previous section, we calculate the energy distribution of non-

thermal electrons by Eq. (4) and synchrotron radiation. We use $\epsilon_e = 10^{-1}$, $\epsilon_B = 10^{-2}$ for both the GRBs and the SNe models for simplicity. Meanwhile, we adopted $p = 2.5$ for the GRBs (Sari et al. 1998) and $p = 3.0$ for the SNe model (Chevalier et al. 2006).

The radio SNe are suppressed by SSA in the early stage of the evolution. As the shock wave expands, the SSA frequency shifts to the lower frequency due to the decrease in the number density and magnetic field strength. The radio flux peaks when the SSA frequency ν_a passes the radio frequency: $\nu_{\text{obs}} = \nu_a$.

The GRBs radio afterglow is also affected by SSA in the early phase of the evolution, then ν_a decreases as the shock wave expands. However, the evolution of radio flux is different from radio SNe due to the large synchrotron peak frequency $\nu_m > \nu_a$. The radio flux becomes maximum when the peak frequency ν_m passes the radio frequency: $\nu_{\text{obs}} = \nu_m$. The radio spectrum evolution strongly depends on the cooling frequency ν_c . The radio flux reaches a local minimum when the spectrum changes from the fast cooling to the slow cooling regime at $\nu_c = \nu_m$ (e.g., Fraija et al. 2022; Wei et al. 2023). However, Sari et al. (1998) shows that the radio flux does not reach the local minimum in the same regime. These inconsistencies may arise from different assumptions about the particle energy distribution. Therefore, the radio afterglow light curves around the local minimum may not be realistic.

Since the peak time of the GRB radio afterglow strongly depends on the shock dynamics and geometry due to the relativistic Doppler effect (Lamb & Kobayashi 2017; Ryan et al. 2020), we focus mainly on the diversity of radio afterglow light curves in a wide range of isotropic equivalent energy E_{iso} and viewing angle θ_{obs} in the following discussion.

3.1. Dependence of isotropic-equivalent energy

Firstly in Figure 2, we illustrate the radio light curve models in which the components of radio SN and GRB afterglow are superimposed. Here we adopt the CSM density scale of $A = 1$, which is derived from the mass-loss rate and wind velocity of Wolf-Rayet stars observed in the Milky Way (Nugis & Lamers 2000). We calculate light curves of the GRB radio afterglow for a wide range of isotropic-equivalent jet energy $E_{\text{iso}} = 10^{50} \sim 10^{55}$ erg. We fix the viewing angle as $\theta_{\text{obs}} = 0.8$ rad.

The peak time of the radio afterglow follows as $\propto E_{\text{iso}}^{1/3}$ for the case in which the shock decelerates following the BM solution in a wind medium (Gao et al. 2013). In the case of $E_{\text{iso}} = 10^{50}$ erg, the afterglow peak time is ~ 10 times shorter than the SN peak time, resulting in a double-peaked light curve (first peak: GRB \rightarrow

second peak: SN). For the $E_{\text{iso}} = 10^{51}$ and 10^{52} erg cases, the peak times of both SN and GRB are comparable, and the resultant light curve becomes a single peak. For $E_{\text{iso}} = 10^{53}$ erg, the 1.43 GHz light curve has a single peak, but the 4.86 GHz and the 8.46 GHz are double-peaked. We denote such light curves as "partially double-peaked" in the following. For $E_{\text{iso}} \geq 10^{54}$ erg, the afterglow peak time becomes more than 10 times longer than the SN peak time, generating a clear double-peaked light curve (first peak: SN \rightarrow second peak: GRB).

3.2. Dependence of viewing angle

The peak time of the radio afterglow also has a strong dependence on the viewing angle θ_{obs} , which is $\propto (\theta_{\text{obs}}/\theta_{\text{jet}} - 1)^{8/3}$ (Lamb & Kobayashi 2017) for the non-spreading approximation. Although the lateral spreading may make the peak time shorter, GRB-SN with a larger viewing angle tends to be a double-peaked radio light curve. Figure 3 shows the superimposed radio light curve for $A = 1$ against the wide range of viewing angle $\theta_{\text{obs}} = 0.0 \sim 1.5$ rad and fixed isotropic-equivalent jet energy as $E_{\text{iso}} = 10^{53}$ erg for GRB radio afterglow.

For a small viewing angle ($\theta_{\text{obs}} < 0.5$ rad, or $\theta_{\text{obs}}/\theta_{\text{jet}} < 10$), the radio SN is overwhelmed by the afterglow component, producing a single-peaked light curve. As the viewing angle increases, the afterglow peak time and flux become longer and decrease, respectively, while the SN component remains unchanged. As a result, the radio light curve becomes partially double-peaked, with the radio SN component emerging around $O(10)$ days. For larger viewing angle ($\theta_{\text{obs}} > 1.2$ rad, or $\theta_{\text{obs}}/\theta_{\text{jet}} > 24$), the afterglow peak time becomes $O(100)$ days, generating a clear double-peaked light curve (first peak: SN \rightarrow second peak: GRB).

3.3. Identification of GRB-SN

The peak time of the radio SNe and GRB afterglow also depends on the density of the wind bubble. Since the radio SN light curve has peaked at $\nu_{\text{obs}} = \nu_a$, the peak time becomes longer for larger A . However, the radio afterglow has peaked at $\nu_{\text{obs}} = \nu_m$. Then, the peak time becomes shorter for the larger A . Thus, double-peaked radio light curves for large A can be produced when the isotropic-equivalent energy E_{iso} and the viewing angle θ_{obs} are large (first peak: SN \rightarrow second peak: GRB), or both are significantly small (first peak: GRB \rightarrow second peak: SN).

Combining the above results, we classify the conditions of a single- or double-peaked light curve in the $(E_{\text{iso}}, \theta_{\text{obs}})$ plane. Figure 4 is the characteristic planes for the cases of $A = 1$ and $A = 10$. We classified radio

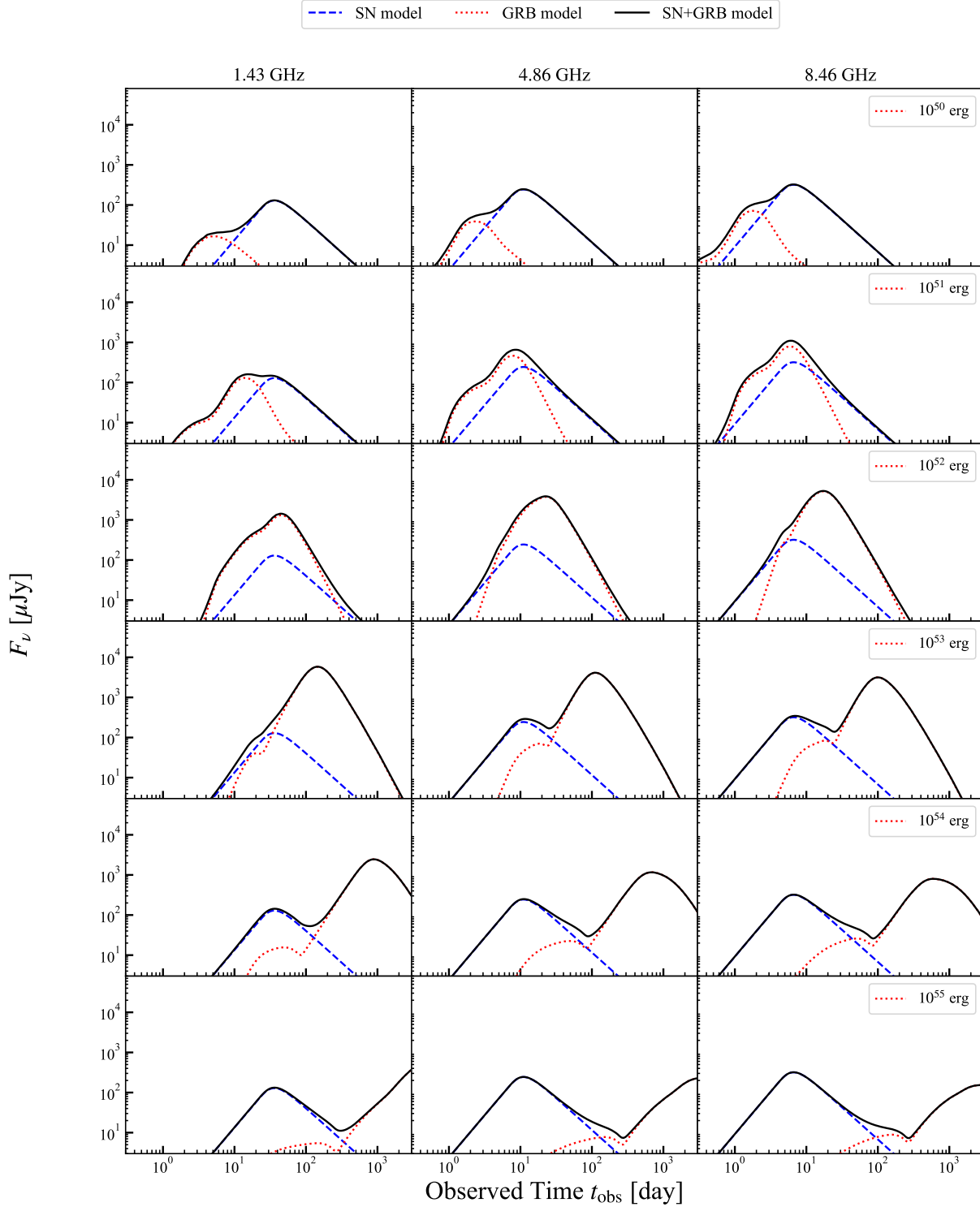


Figure 2. Demonstrative superposition of radio light curves (solid) of an SN (dashed) and a GRB afterglow (dotted) for fixed viewing angle $\theta_{\text{obs}} = 0.8$ rad. From the top to the bottom, the isotropic-equivalent energy is changed as $E_{\text{iso}} = 10^{50}, 10^{51}, 10^{52}, 10^{53}, 10^{54}, 10^{55}$ erg.

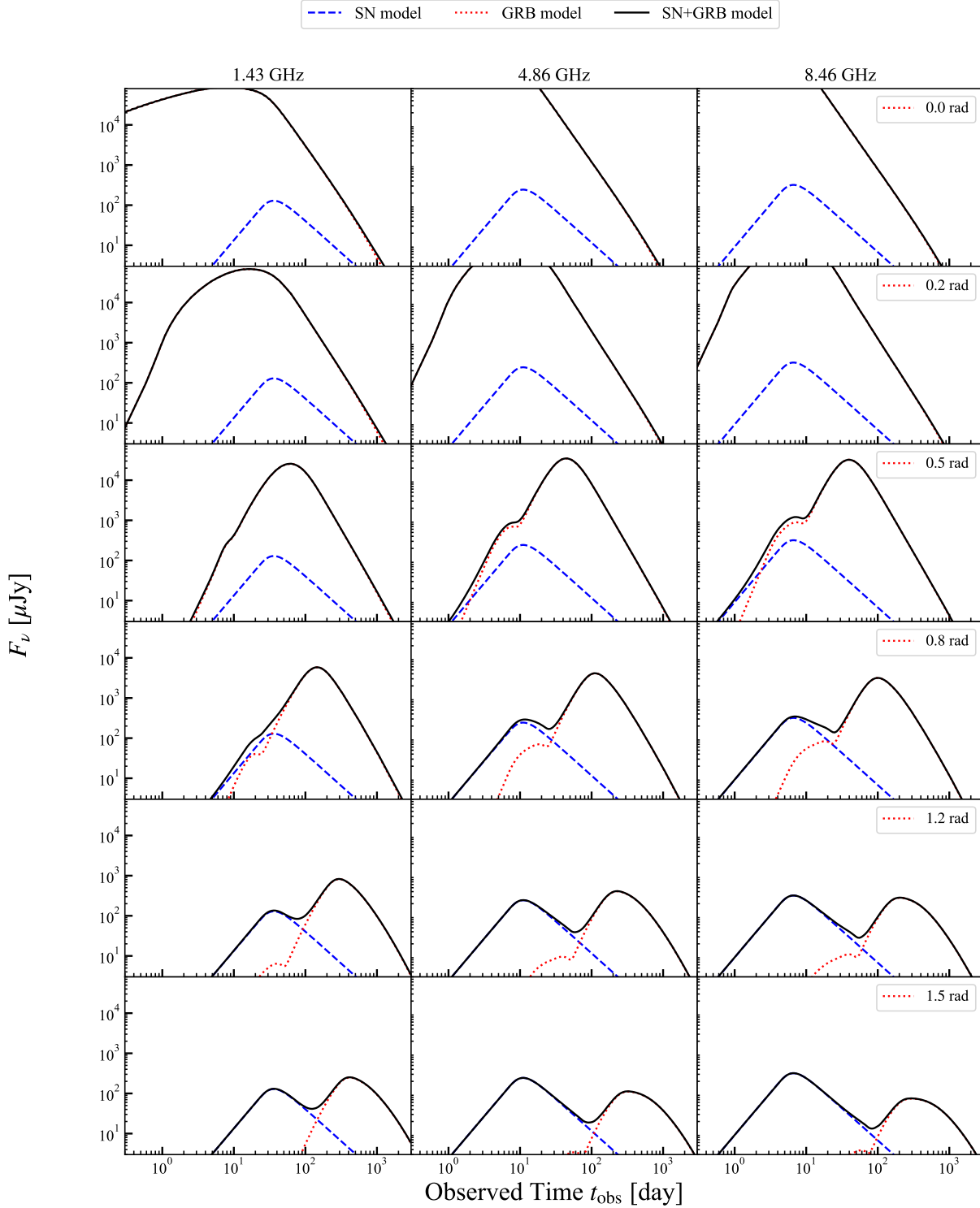


Figure 3. The same as Figure 2, but the isotropic-equivalent energy is fixed to $E_{\text{iso}} = 10^{53}$ erg. From the top to the bottom, the viewing angle is changed as $\theta_{\text{obs}} = 0.0, 0.2, 0.5, 0.8, 1.2, 1.5$ rad.

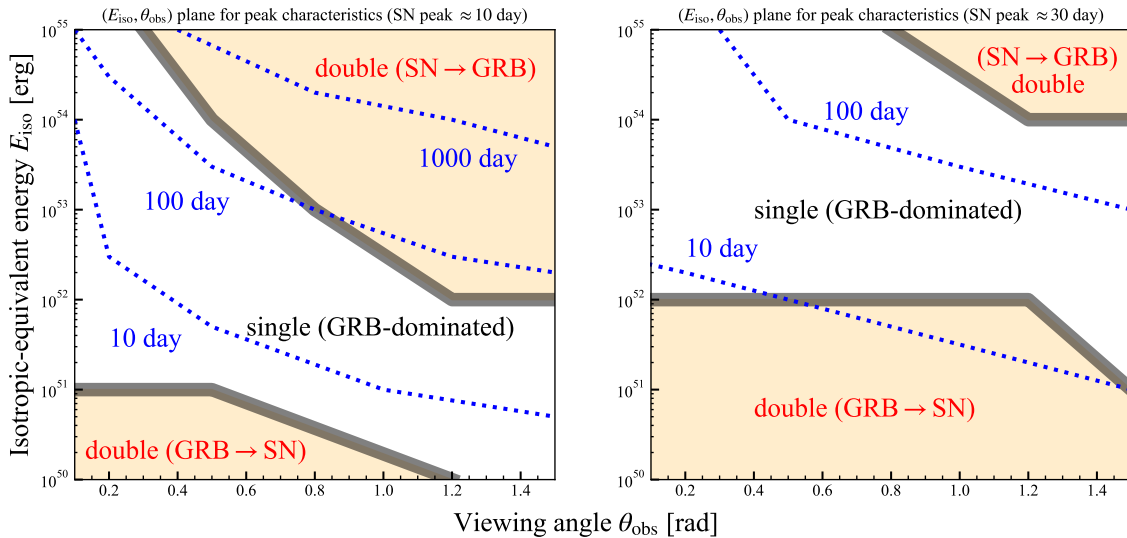


Figure 4. The characteristic $(E_{\text{iso}}, \theta_{\text{obs}})$ plane for $A = 1$ (left panel) and $A = 10$ (right panel). The blue-dotted lines express the typical peak time of the GRB radio afterglow, meanwhile the typical SN peak is around 10 days. The black shaded regions corresponds to ‘partial’ cases.

light curves as “double” when it has clear double peak in all 1.43, 4.86, and 8.46 GHz bands and as “single” when it has no double peak in all of them. Otherwise, we classified them as “partial”.

We find that the double peak radio light curve whose peaks are at $\mathcal{O}(10)$ days (SNe) and $\mathcal{O}(100)$ days (GRBs) are likely formed when the angle ratio $\theta_{\text{obs}}/\theta_{\text{jet}}$ is greater than ~ 10 for the typical GRBs with the isotropic-equivalent energy $E_{\text{iso}} = 10^{52} \sim 10^{53}$ erg for the case of $A = 1$, and much larger E_{iso} for the case of $A = 10$. If E_{iso} is significantly large (say more than 10^{54} erg), the typical peak time of the GRB radio afterglow can be $\mathcal{O}(1000)$ days. Thus, the follow-up observation of radio SNe in a few years later might find off-axis GRBs with significantly high E_{iso} comparable to GRB 221009A (LHAASO Collaboration et al. 2023).

On the other hand, we also find that the double peak radio light curve whose peaks are at $\mathcal{O}(1)$ days (GRBs) and $\mathcal{O}(10)$ days (SNe) are likely formed when the isotropic-equivalent energy E_{iso} is less than 10^{52} erg, but almost independent of the angle ratio $\theta_{\text{obs}}/\theta_{\text{jet}}$. Thus, rapid follow-up of radio observation for Ic-BL SNe might find the off-axis low-luminosity GRBs.

4. SUMMARY AND DISCUSSION

The discovery of SN 1998bw associated with GRB 980425 has confirmed that a Type IcBL SN is a plausible candidate for the progenitor of long GRBs. However, it is also recognized that the clear association between long GRBs and Type IcBL SNe has been confirmed for only a limited number of samples, which has invoked ex-

ploration for the causes. One of the probable explanations is that we are missing off-axis GRBs accompanying Type IcBL SNe, that launch jets in the direction away from us. Radio observations have been examined to give constraints on probable associations of long GRBs and Type IcBL SNe, while there have been seldom attempts to comprehensively predict the morphology of the radio light curve in GRB-SNe. In this research, we construct a model for radio light curves of GRB-SNe as a composite of contributions from radio SN and GRB afterglow. We survey the wide ranges of the isotropic-equivalent energy and viewing angle to cover parameter spaces reproducing low-luminosity GRBs and off-axis GRBs. We find the contribution of off-axis GRBs afterglow can produce double-peaked radio light curves of GRB-SNe in specific parameter spaces, the properties of which are described as follows.

1. The large isotropic-equivalent energy $E_{\text{iso}} > 10^{53}$ erg or the large viewing angle ratio $\theta_{\text{obs}}/\theta_{\text{jet}} > 10$ leads to a double-peaked radio light curve, whose first and second peak can originate from SNe and GRBs, respectively.
2. The small isotropic-equivalent energy $E_{\text{iso}} < 10^{52}$ erg leads to a double-peaked radio light curve almost independent of the viewing angle θ_{obs} , whose first and second peak can originate from GRBs and SNe, respectively.

It would be useful for us to describe how to tell from which radio-emitting source each peak in the double-peaked light curve is characterized. It would be worth

noting that the decay rates of the GRB afterglow are more rapid than that of the radio SN component, as demonstrated in Figure 2 and 3. This is caused by the rapid deceleration rate of the GRB jet in the Sedov-Taylor phase observed in the late phase. We suppose that the measurement of the decay rate would be a key to discriminating the radio-emitting source between radio SN and GRB afterglow.

In this study, we have neglected a contribution from a counter jet. As the viewing angle θ_{obs} becomes large, the counter jet radiation may increase the radio flux. A small bump might be created in the radio light curve after the peak of the radio afterglow. At $\theta_{\text{obs}} = \pi/2$, the radio afterglow flux becomes twice. Other effects such as structured jet (e.g., Ryan et al. 2020; Obayashi et al. 2024) might also affect the late-phase radio afterglow, but we leave these problems in future studies.

Finally, we mention the assumption of microphysics parameters ϵ_e and ϵ_B imposed in this study. For the purpose of demonstration, we have just assumed that the values of ϵ_e and ϵ_B are equal between radio SN and GRB afterglow each other without introducing any time dependence. Although the exact values of these microphysics parameters are still unknown, it should be noted that lower values of ϵ_e are also inferred from previous works (Duncan et al. 2023). Asano (2024) demonstrated modeling for GRB afterglows with decaying ϵ_e and ϵ_B introduced to reproduce typical X-ray afterglow light curves. These effects may be significant in the practical

fitting of double-peaked radio light curves of GRB-SNe obtained in the future.

According to our results, the radio light curve of a Type IcBL SN with an off-axis GRB event can be diverse more than expected before. The second peak can appear on a much longer time scale than the first peak, as demonstrated in Figure 2 and 3. Contrary to this prediction, radio follow-up observations of Type IcBL SNe have been typically limited within 1 year after the explosion and seldom covered the observational time range for more than a few years; it is just recently that the importance of late-phase follow-up radio observations of radio SNe has been recognized in the perspective of rebrightening (Rose et al. 2024). We suggest that long-term monitoring of Type Ic-BL SNe allows us to examine the universality of the presence of GRB jets, serving as a clue to understanding the nature of GRB-SN progenitors.

The authors thankfully acknowledge the computer resources provided by the Institute for Cosmic Ray Research (ICRR), the University of Tokyo. This work is supported by the joint research program of ICRR, JSPS KAKENHI Grant Numbers JP23KJ0692 (Y.K.) and 21K13964 (R.S.), the National Science and Technology Council, Taiwan under grant No. MOST 110-2112-M-001-068-MY3, and the Academia Sinica, Taiwan under a career development award under grant No. AS-CDA-111-M04 (T.M.).

REFERENCES

- Aharonian, F. A., Kelner, S. R., & Prosekin, A. Y. 2010, *PhRvD*, 82, 043002, doi: [10.1103/PhysRevD.82.043002](https://doi.org/10.1103/PhysRevD.82.043002)
- Asano, K. 2024, *ApJ*, 970, 141, doi: [10.3847/1538-4357/ad6148](https://doi.org/10.3847/1538-4357/ad6148)
- Asano, K., Takahara, F., Kusunose, M., Toma, K., & Kakuwa, J. 2014, *ApJ*, 780, 64, doi: [10.1088/0004-637X/780/1/64](https://doi.org/10.1088/0004-637X/780/1/64)
- Asano, K., & Terasawa, T. 2009, *ApJ*, 705, 1714, doi: [10.1088/0004-637X/705/2/1714](https://doi.org/10.1088/0004-637X/705/2/1714)
- Bell, A. R. 1978, *MNRAS*, 182, 147, doi: [10.1093/mnras/182.2.147](https://doi.org/10.1093/mnras/182.2.147)
- Björnsson, C. I. 2022, *ApJ*, 936, 98, doi: [10.3847/1538-4357/ac87aa](https://doi.org/10.3847/1538-4357/ac87aa)
- Blandford, R. D., & McKee, C. F. 1976, *Physics of Fluids*, 19, 1130, doi: [10.1063/1.861619](https://doi.org/10.1063/1.861619)
- Blandford, R. D., & Ostriker, J. P. 1978, *ApJL*, 221, L29, doi: [10.1086/182658](https://doi.org/10.1086/182658)
- Cano, Z., Wang, S.-Q., Dai, Z.-G., & Wu, X.-F. 2017, *Advances in Astronomy*, 2017, 8929054, doi: [10.1155/2017/8929054](https://doi.org/10.1155/2017/8929054)
- Chevalier, R. A. 1982a, *ApJ*, 259, 302, doi: [10.1086/160167](https://doi.org/10.1086/160167)
- . 1982b, *ApJ*, 258, 790, doi: [10.1086/160126](https://doi.org/10.1086/160126)
- Chevalier, R. A., & Fransson, C. 1994, *ApJ*, 420, 268, doi: [10.1086/173557](https://doi.org/10.1086/173557)
- . 2017, in *Handbook of Supernovae*, ed. A. W. Alsabti & P. Murdin, 875, doi: [10.1007/978-3-319-21846-5_34](https://doi.org/10.1007/978-3-319-21846-5_34)
- Chevalier, R. A., Fransson, C., & Nymark, T. K. 2006, *ApJ*, 641, 1029, doi: [10.1086/500528](https://doi.org/10.1086/500528)
- Corsi, A., Gal-Yam, A., Kulkarni, S. R., et al. 2016, *ApJ*, 830, 42, doi: [10.3847/0004-637X/830/1/42](https://doi.org/10.3847/0004-637X/830/1/42)
- Duffell, P. C., & Laskar, T. 2018, *ApJ*, 865, 94, doi: [10.3847/1538-4357/aadb9c](https://doi.org/10.3847/1538-4357/aadb9c)
- Duncan, R. A., van der Horst, A. J., & Beniamini, P. 2023, *MNRAS*, 518, 1522, doi: [10.1093/mnras/stac3172](https://doi.org/10.1093/mnras/stac3172)
- Fan, Y., & Piran, T. 2006, *MNRAS*, 369, 197, doi: [10.1111/j.1365-2966.2006.10280.x](https://doi.org/10.1111/j.1365-2966.2006.10280.x)

- Finneran, G., Cotter, L., & Martin-Carrillo, A. 2024, arXiv e-prints, arXiv:2411.08866, doi: [10.48550/arXiv.2411.08866](https://doi.org/10.48550/arXiv.2411.08866)
- Fouka, M., & Ouichaoui, S. 2013, *Research in Astronomy and Astrophysics*, 13, 680, doi: [10.1088/1674-4527/13/6/007](https://doi.org/10.1088/1674-4527/13/6/007)
- Fraija, N., Galvan-Gamez, A., Betancourt Kamenetskaia, B., et al. 2022, *ApJ*, 940, 189, doi: [10.3847/1538-4357/ac68e1](https://doi.org/10.3847/1538-4357/ac68e1)
- Fransson, C., & Björnsson, C.-I. 1998, *ApJ*, 509, 861, doi: [10.1086/306531](https://doi.org/10.1086/306531)
- Galama, T. J., Vreeswijk, P. M., van Paradijs, J., et al. 1999, *A&AS*, 138, 465, doi: [10.1051/aas:1999311](https://doi.org/10.1051/aas:1999311)
- Gao, H., Lei, W.-H., Zou, Y.-C., Wu, X.-F., & Zhang, B. 2013, *NewAR*, 57, 141, doi: [10.1016/j.newar.2013.10.001](https://doi.org/10.1016/j.newar.2013.10.001)
- Giannios, D., Mimica, P., & Aloy, M. A. 2008, *A&A*, 478, 747, doi: [10.1051/0004-6361:20078931](https://doi.org/10.1051/0004-6361:20078931)
- Granot, J. 2005, *ApJ*, 631, 1022, doi: [10.1086/432676](https://doi.org/10.1086/432676)
- Granot, J., Panaitescu, A., Kumar, P., & Woosley, S. E. 2002, *ApJL*, 570, L61, doi: [10.1086/340991](https://doi.org/10.1086/340991)
- Izzo, L., Auchettl, K., Hjorth, J., et al. 2020, *A&A*, 639, L11, doi: [10.1051/0004-6361/202038152](https://doi.org/10.1051/0004-6361/202038152)
- Keshet, U., & Waxman, E. 2005, *PhRvL*, 94, 111102, doi: [10.1103/PhysRevLett.94.111102](https://doi.org/10.1103/PhysRevLett.94.111102)
- Kobayashi, S., & Sari, R. 2000, *ApJ*, 542, 819, doi: [10.1086/317021](https://doi.org/10.1086/317021)
- Kulkarni, S. R., Frail, D. A., Wieringa, M. H., et al. 1998, *Nature*, 395, 663, doi: [10.1038/27139](https://doi.org/10.1038/27139)
- Kusafuka, Y., & Asano, K. 2024, *MNRAS*, 536, 1822, doi: [10.1093/mnras/stae2734](https://doi.org/10.1093/mnras/stae2734)
- Kusafuka, Y., Asano, K., Ohmura, T., & Kawashima, T. 2023, *MNRAS*, 526, 512, doi: [10.1093/mnras/stad2804](https://doi.org/10.1093/mnras/stad2804)
- Lamb, G. P., & Kobayashi, S. 2017, *MNRAS*, 472, 4953, doi: [10.1093/mnras/stx2345](https://doi.org/10.1093/mnras/stx2345)
- LHAASO Collaboration, Cao, Z., Aharonian, F., et al. 2023, *Science*, 380, 1390, doi: [10.1126/science.adg9328](https://doi.org/10.1126/science.adg9328)
- MacFadyen, A. I., Woosley, S. E., & Heger, A. 2001, *ApJ*, 550, 410, doi: [10.1086/319698](https://doi.org/10.1086/319698)
- Maeda, K. 2012, *ApJ*, 758, 81, doi: [10.1088/0004-637X/758/2/81](https://doi.org/10.1088/0004-637X/758/2/81)
- Maeda, K., Chandra, P., Matsuoka, T., et al. 2021, *ApJ*, 918, 34, doi: [10.3847/1538-4357/ac0dbc](https://doi.org/10.3847/1538-4357/ac0dbc)
- Matsuoka, T., Kimura, S. S., Maeda, K., & Tanaka, M. 2024, *ApJ*, 960, 70, doi: [10.3847/1538-4357/ad096c](https://doi.org/10.3847/1538-4357/ad096c)
- Matsuoka, T., Maeda, K., Lee, S.-H., & Yasuda, H. 2019, *ApJ*, 885, 41, doi: [10.3847/1538-4357/ab4421](https://doi.org/10.3847/1538-4357/ab4421)
- Mimica, P., Giannios, D., & Aloy, M. A. 2009, *A&A*, 494, 879, doi: [10.1051/0004-6361:200810756](https://doi.org/10.1051/0004-6361:200810756)
- Nugis, T., & Lamers, H. J. G. L. M. 2000, *A&A*, 360, 227
- Obayashi, K., Toriyama, A., Murakoshi, M., et al. 2024, *Journal of High Energy Astrophysics*, 41, 1, doi: [10.1016/j.jheap.2023.12.001](https://doi.org/10.1016/j.jheap.2023.12.001)
- Ostriker, J. P., & McKee, C. F. 1988, *Reviews of Modern Physics*, 60, 1, doi: [10.1103/RevModPhys.60.1](https://doi.org/10.1103/RevModPhys.60.1)
- Palliyaguru, N. T., Corsi, A., Pérez-Torres, M., Varenius, E., & Van Eerten, H. 2021, *ApJ*, 910, 16, doi: [10.3847/1538-4357/abelc9](https://doi.org/10.3847/1538-4357/abelc9)
- Pang, S.-L., & Dai, Z.-G. 2024, *MNRAS*, 528, 2066, doi: [10.1093/mnras/stae197](https://doi.org/10.1093/mnras/stae197)
- Ramirez-Ruiz, E., Celotti, A., & Rees, M. J. 2002, *MNRAS*, 337, 1349, doi: [10.1046/j.1365-8711.2002.05995.x](https://doi.org/10.1046/j.1365-8711.2002.05995.x)
- Rhoads, J. E. 1999, *ApJ*, 525, 737, doi: [10.1086/307907](https://doi.org/10.1086/307907)
- Rose, K., Horesh, A., Murphy, T., et al. 2024, *MNRAS*, 534, 3853, doi: [10.1093/mnras/stae2289](https://doi.org/10.1093/mnras/stae2289)
- Rossi, E., Lazzati, D., & Rees, M. J. 2002, *MNRAS*, 332, 945, doi: [10.1046/j.1365-8711.2002.05363.x](https://doi.org/10.1046/j.1365-8711.2002.05363.x)
- Ryan, G., van Eerten, H., Piro, L., & Troja, E. 2020, *ApJ*, 896, 166, doi: [10.3847/1538-4357/ab93cf](https://doi.org/10.3847/1538-4357/ab93cf)
- Salas, P., Bauer, F. E., Stockdale, C., & Prieto, J. L. 2013, *MNRAS*, 428, 1207, doi: [10.1093/mnras/sts104](https://doi.org/10.1093/mnras/sts104)
- Sari, R., & Piran, T. 1995, *ApJL*, 455, L143, doi: [10.1086/309835](https://doi.org/10.1086/309835)
- Sari, R., Piran, T., & Narayan, R. 1998, *ApJL*, 497, L17, doi: [10.1086/311269](https://doi.org/10.1086/311269)
- Sironi, L., Petropoulou, M., & Giannios, D. 2015, *MNRAS*, 450, 183, doi: [10.1093/mnras/stv641](https://doi.org/10.1093/mnras/stv641)
- Sironi, L., & Spitkovsky, A. 2011, *ApJ*, 726, 75, doi: [10.1088/0004-637X/726/2/75](https://doi.org/10.1088/0004-637X/726/2/75)
- Soderberg, A. M., Nakar, E., Berger, E., & Kulkarni, S. R. 2006, *ApJ*, 638, 930, doi: [10.1086/499121](https://doi.org/10.1086/499121)
- Soderberg, A. M., Chakraborti, S., Pignata, G., et al. 2010, *Nature*, 463, 513, doi: [10.1038/nature08714](https://doi.org/10.1038/nature08714)
- Suzuki, A., & Maeda, K. 2018, *MNRAS*, 478, 110, doi: [10.1093/mnras/sty999](https://doi.org/10.1093/mnras/sty999)
- Truelove, J. K., & McKee, C. F. 1999, *The Astrophysical Journal Supplement Series*, 120, 299, doi: [10.1086/313176](https://doi.org/10.1086/313176)
- van den Bergh, S., & Tammann, G. A. 1991, *ARA&A*, 29, 363, doi: [10.1146/annurev.aa.29.090191.002051](https://doi.org/10.1146/annurev.aa.29.090191.002051)
- van der Horst, A. J., Kamble, A. P., Paragi, Z., et al. 2011, *ApJ*, 726, 99, doi: [10.1088/0004-637X/726/2/99](https://doi.org/10.1088/0004-637X/726/2/99)
- van Eerten, H. 2014, *MNRAS*, 442, 3495, doi: [10.1093/mnras/stu1025](https://doi.org/10.1093/mnras/stu1025)
- van Eerten, H. J., & MacFadyen, A. I. 2012, *ApJ*, 751, 155, doi: [10.1088/0004-637X/751/2/155](https://doi.org/10.1088/0004-637X/751/2/155)
- Wang, L., & Wheeler, J. C. 1998, *ApJL*, 504, L87, doi: [10.1086/311580](https://doi.org/10.1086/311580)
- Waxman, E. 1997, *ApJL*, 491, L19, doi: [10.1086/311057](https://doi.org/10.1086/311057)
- Wei, Y., Zhang, B. T., & Murase, K. 2023, *MNRAS*, 524, 6004, doi: [10.1093/mnras/stad2122](https://doi.org/10.1093/mnras/stad2122)

Woods, E., & Loeb, A. 1999, *ApJ*, 523, 187,
doi: [10.1086/307738](https://doi.org/10.1086/307738)

Woosley, S. E., & Bloom, J. S. 2006, *ARA&A*, 44, 507,
doi: [10.1146/annurev.astro.43.072103.150558](https://doi.org/10.1146/annurev.astro.43.072103.150558)

Young, D. R., Smartt, S. J., Valenti, S., et al. 2010, *A&A*,
512, A70, doi: [10.1051/0004-6361/200913004](https://doi.org/10.1051/0004-6361/200913004)